JKAU: Env. Design Sci., **Vol. 15,** pp: 93 - 111 (2024)
DOI: 10.4197 / Env.15-4

Urban Thermal Vulnerability Mapping for Climate Mitigation: A Case from a Coastal Megacity in Saudi Arabia

Ahmad Maghrabi

Faculty of Architecture and Planning, King Abdulaziz University, Jeddah, Saudi Arabia

amaghrabi84@gmail.com

Abstract. Rapid urban expansion is considerably affecting urban surface properties through the substitution of natural landscapes with impervious surface areas. These alterations considerably affect the thermal properties of urban landscapes and increase urban heat island (UHI) intensity and thermal vulnerability; therefore, mapping the thermal vulnerability to mitigate public health concerns is essential. In this study, we mapped the thermal vulnerability of the Jeddah megacity in Saudi Arabia by using principal component analysis (PCA) and a fuzzy analytical hierarchy process (fuzzy-AHP) model. We also conducted correlation and regression anal-yses to understand the relationships and impacts of the remote-sensing indices on thermal vulnerability. The results showed that from 2000 to 2020, built-up land, water bodies, and open land increased by approxi-mately 50%, 4.46%, and 14.11%, respectively. We found that the south-eastern parts of the city were highly vulnerable according to the thermal vulnerability map. In both models, 73.64% (PCA-based model) and 57.29% (fuzzy-AHP-based model) of the city were characterized as thermally vulnerable zones. In our correlation results, we showed that ecological parameters, such as the normalized difference vegetation (NDVI) and moisture indices (NDMI), as well as wetness, had negative correlations with urban thermal vulnerability, while the correlations for land surface temperature (LST) and the urban thermal field variance index (UTFVI) were positive. Thus, in this study, we constructed an effective framework for climate mitigation strategies that can be used to reduce urban thermal or heat vulnerability.

Keywords: Heat vulnerability, Jeddah megacity, Principal component analysis, Public health, Climate miti-gation.

1. Introduction

Thermal vulnerability is the degree to which a system and it sub-systems are likely to be suffered due to heat hazards. The thermal vulnerability is affected by a series of factors such as land surface temperature (LST), normalized difference vegetation index (NDVI), urban surface characteristics, and population density [1]. The physical components such as land surface coverage, building, and urban density are the most prominent factor affecting thermal vulnerability. In previous literatures, both physical and social factors were mixed to develop thermal vulnerability framework [2, 3, 4, 5]. The physical components have direct impact on the thermal vulnerability whereas social components have indirect impact on the thermal vulnerability adaptation [6,7]. Therefore, it is essential to develop thermal vulnerability framework on the basis of the physical components.

Rapid rates of urbanization have produced a series of environmental problems and have considerably affected landscape compositions, energy balances, and water budgets [8, 9]. Alterations to land

surface properties have resulted in changes in thermal characteristics [10, 11]. Natural land surfaces, such as forest cover, water bodies, and agricultural regions, are replaced by impervious artificial and semi-natural surface areas due to rapid urban expansion [12, 13, 14, 15, 16]. The resulting increases in land surface temperature (LST) cause the emergence of urban heat islands (UHIs) [17, 18]. In cities, the UHI effect results in various health-related diseases, particularly for residents living without air-conditioning systems [19, 20]. An increase in extreme temperature causes indoor and outdoor discomfort, reduces work performance, and increases morbidity and mortality [21, 22, 23]. The effects of extreme temperatures vary depending on the cities examined because of differences in their surface properties and socio-economic conditions [24, 3]. Therefore, we need to understand thermal vulnerability for climate change adaptation and mitigation strategies. In cities, thermal vulnerability is largely affected by urban geophysical settings, such as the vegetation cover, built-up density, urban morphology, and socio-economic and demographic factors [25,17]. Previously, thermal vulnerability was assessed based on socio-economic and demographic factors, such as age, gender, education, and health [26, 18]. However, researchers have been undertaking quantitative and qualitative approaches to map thermal vulnerability in cities, focusing on socio-demographic and biophysical properties [27]. Remote-sensing-based biophysical parameters, such as land use and land cover (LULC) maps, NDVI and built-up (NDBI) indices, and LST have been widely used to develop heat vulnerability mapping [28, 29, 30, 31]. Therefore, remote-sensing-based indices have immense potential for our development and understanding of reliable information regarding thermal vulnerability mapping. The application of remote-sensing-based indices to develop thermal vulnerability mapping has several advantages [32, 33, 34, 35]. First, remote-sensing-based indices can be used for large areas and display high effectiveness in mapping land surface features. Second, images of a medium resolution can effectively detect the variation in the land surface composition at a local scale, even in complex urban systems. Despite this, the process of remote-sensing-based detection regarding thermal vulnerability has remained generalized because of low spatial resolutions. Regardless of this limitation, remote-sensing-based thermal vulnerability maps can considerably contribute toward the mitigation of climate change. In previous studies, researchers used several remote sensing indices to construct urban thermal vulnerability (UTV) mapping. Generally, NDVI was combined with socio-economic parameters to develop an UTV index [36, 37]. In this study, we used combined remote sensing indices to construct a composite UTV map in the Jeddah megacity. Through our combination of these indices, we clearly detected the greenness, wetness, and heat across the city.

The LST has considerably increased over the last few decades due to rapid urban expansion and dramatic increases in impervious surface areas [38, 39, 40]. The spatial distribution of the LST is determined by several factors across a city

[41, 42]. For example, the conversion of natural land-cover types (such as water bodies and vegetation cover) into built-up areas and other land-use types considerably affects the energy balance [43, 44, 45, 46, 47]. Thus, global warming due to the emission of greenhouse gases (GHGs) has become one of the most serious global-scale challenges in the fight against climate change [48]. One of the prominent impacts of global and regional climate change is heat waves [49, 50]. Lemonsu et al. [51] argued that heat waves across the globe are likely to be the most frequent climatic event at the end of the century (one event/year), and they will increase in the future. The extreme heat events in cities have become a growing concern, as the urban heat island (UHI) effect emerges due to high temperatures during heat waves [52, 53]. Thus, a recent study concerning heat vulnerability in cities was conducted [54]. In particular, in hot desert regions, an assessment of UTV is essential for the alleviation of public health concerns and to achieve urban-environment-health sustainability.

Therefore, we examined the patterns of thermal vulnerability displayed by our study of the Jeddah megacity in Saudi Arabia. Jeddah megacity has experienced rapid rate of urbanization and, thus rapid urban expansion leads to the increase of the impervious surfaces. In previous studies, it was well documented that the impervious surface play significant role to increase LST and promote thermal vulnerability [55]. Through conducting a literature review, we identified notable research gaps. First, most studies were performed with a focus on the LST and land use and land cover change (LULC) mapping [56, 57]. Second, in Saudi Arabia, cities are growing rapidly, which has considerably affected urban landscapes by altering the surface properties. However, to the best of our knowledge, no study has been carried out to understand the impact of this alteration on the thermal pattern. Third, the Earth has undergone considerable climate change and the effects of this process are expected to increase in the future [58, 59]. However, research regarding this issue is lacking in the Saudi Arabian context. Therefore, we focused on the thermal mapping of Saudi Arabian cities for climate change mitigations. In this study, we developed a thermal vulnerability map of the Jeddah megacity by using remote sensing indices. Our findings in this study are useful for policymakers regarding the implementation of spatial planning strategies to mitigate climate change.

2. Material and Methods

2.1. About the Study Area

Jeddah is one of the largest megacities in Saudi Arabia and is located on the west coast of the Red Sea. It has a population of about 4 million, with a density of 5400 people per square kilometer. The megacity has a dry and hot desert climate and the average annual rainfall is about 45 mm. The temperature during the summer season climbs above 40 °C and is around 28 °C during the winter [60]. The study area map is presented in Fig. 1.

2.2. Data Source

In this study, we used LANDSAT images to conduct the UTV mapping of the Jeddah megacity for the year 2021. We obtained the LANDSAT 8 OLI (Operational land imager) images from the United State Geological Survey (USGS),

with the numbers of paths and rows being 170 and 045, respectively (Table 1). We downloaded the cloud-free images for land-use and land-cover classification and the construction of biophysical indices from United State Geological Survey (USGS). The satellite images were downloaded to develop land use and land cover (LULC) maps and indices related to the thermal vulnerability. The pixel based classification approach (maximum likelihood classification has been applied to develop LULC maps. The LULC maps have been categorized into four classes, namely- Built-up areas, vegetation cover, open land and water bodies, respectively. The accuracy assessments of the classified LULC maps were also done using Kappa statistics with an average accuracy of 82.5% (79.25% in 2000, and 80.28% in 2021). The LUC maps and bio-physical indices maps were developed in ArcGIS environment.

2.3. Selection of Parameters

In this study, we used nine remote-sensing parameters to develop a thermal vulnerability map of the Jeddah megacity: wetness; normalized difference vegetation (NDVI), moisture (NDMI), impervious (NDII), soil (NDSI), and impervious surface indices (NDISI); the urban thermal field variance index (UTFVI), the temperature condition index (TCI); and the LST. These remote indices are closely linked to urban surface properties. For example, increases in the LST correspond to increasing impervious surface and decreasing normalized difference vegetation indices in urban areas. In previous studies, these indices were widely used to develop heat vulnerability framework [61, 62]. Therefore, we focused on these remote-sensing-based indices to study the thermal patterns in the Jeddah megacity. The details of the indices have been discussed in Table 2. The indices selected to develop thermal vulnerability had immense impact on the thermal pattern. For example, LST had very strong positive impact on the thermal behavior pattern of the city. The areas with high LST are characterized by high UHIeffect and thermally more vulnerable. On the other hand, the areas with high NDVI are characterized by lowerLST and lower thermal vulnerability. Thus, these parameters have significant impact on the thermal vulnerability in the city [52, 53]. The spatial variability of the thermal patterns is largely affected by these bio-physical parameters.

2.4. Methodology

We developed a composite thermal vulnerability index to obtain the spatial thermal patterns in the city. We applied a grid-based approach to extract the remote sensing data from each index. We created a total of 169 grids over the entire city, from which we extracted index values. Finally, we aggregated the indices to develop a composite thermal vulnerability mapping of the city.

2.4.1. Normalization of the Parameters

In this study, we used several unidirectional and unit-free parameters in various dimensions to develop a composite thermal vulnerability mapping of the Jeddah megacity. Normalization is a crucial multivariate statistical method that is used to avoid large differences in the variances between the datasets [63]. In a previous study, normalization methods were widely used to make the parameters unit-free and unidirectional to discern the

human development index and life expectancy [64]. In this study, we used both positive and negative parameters related to thermal vulnerability. Thus, we used two equations for the normalization of the parameters. These are as follows:

$$\text{Index}Xi = \frac{\text{Xi-Xmin}}{\text{Xmax-Xmin}} \text{ (positive variables)}$$
$$\text{Index}Yi = \frac{\text{Ymax-Yi}}{Ymax - Ymin} \text{ (negative variables)} \quad (1)$$

where IndexXi/Yi is the observed value of indicator i, while $\frac{X_{min}}{Ymin}$ and X_{max} / $Ymax$ indicate the minimum and maximum values within the same array, respectively.

2.4.2. PCA-Based Thermal Vulnerability Mapping

Principal component analysis (PCA) is one of the statistical methods that are applied for the dimension reduction of variables, which involves an orthogonal transformation to convert a set of correlated variables into linearly uncorrelated variables (known as principal components). Mathematically, PCA depends on an eigenvector as the basis of the multivariate analysis [65]. PCA can be performed by using an eigenvalue of the datasets called a correlation matrix. The results of PCA are presented as a component score (also known as a factor score). The PCA method has been widely used as a tool for social [66], ecological [67], and climate vulnerability assessment, as well as for landslide susceptibility [68] and groundwater modeling [69]. Cross-validation can be made through the bootstrapping or jackknife method [56]. Additionally, the number of principal components is identified based on the Kaiser–Meyer–Olkin (KMO) and Bartlett's tests. The KMO test is generally used to determine the sample adequacy and value of the ranges from 0 to 1, and a KMO value of >0.50 is considered to be suitable for PCA. Bartlett's test is applied to measure the level of significance (p-value < 0.5 is considered to be significant).

2.4.3. Fuzzy-Based Thermal Vulnerability Mapping

The remote-sensing-based parameters used to perform composite thermal vulnerability mapping were not of equal importance. Therefore, we need to assign the weight of each parameter to develop the model. The analytical hierarchy process (AHP) is one of the most efficient methods that can be used to assign the weights of the parameters and solve any complex problem. AHPs, such as multicriteria decision making (MCDM), are widely applied in various research fields, such as in landslide [70, 71] and groundwater modeling [72, 73] and in eco-environmental [74] social [75], and climate-change vulnerability modeling [76]. Additionally, AHP is widely used in medical sciences, such as ZIKA and dengue risk modeling [77]. In this method, the weights are provided based on the relative importance of the parameters through a pair-wise comparison [78, 79].

We assigned the weights of the parameters by following the approach proposed by Saaty [78] (1977). We calculated the weights of the corresponding parameters by dividing the cell values and the aggregation of the column values of the comparison matrix. We normalized the weights of the layers by using the

maximum eigenvalues. Consistency ratio (CR) values greater than 0.1 demonstrate the reliability of the model. We used the following equations for the computation of the pair-wise comparison and the CR:

$$A = \begin{matrix} a_{11} & a_{12} & a_{13} & a_{n1} \\ a_{21} & a_{22} & a_{23} & a_{n2} \\ \ldots & \ldots & a_{ij} & \ldots \\ a_{n123} & a_{n} & a_{n} & a_{n} \end{matrix}$$

Where,

$$a_{ij} = \frac{\text{Wi weight for attribute i}}{\text{Wj weight for attribute j}}$$

We calculated the CR by using the following equation:

$$CR = CI/RI$$

where CI and RI denote the consistency and random indices, respectively. where CI can be computed using the following equation:

$$CI = \frac{\lambda_{Max} - n}{n-1}$$

where λ_{Max} refers to the largest eigenvalue and n is the number of layers.

2.5. *Development of the Urban Thermal Vulnerbaility (UTV) Framework*

The biophysical indices related to the vegetation, soil, climatic, and water conditions, as well as the surface characteristics of the urban area have been used to develop an UTV index. These biophysical indices largely control the thermal pattern of an urban area. Vegetation health is detected using the NDVI. There is a negative correlation between the NDVI and land surface temperature, which largely controls the thermal patterns of an area. We used the other indices, such as the NDSI and wetness, for vulnerability analysis. These remote-sensing-based indices were previously used for ecological modeling and vulnerability and risk analysis [80, 81]. The following equation has been used to develop UTV-

$$\text{UTV} = P_{11} W_{11} + P_{21} W_{21} \ldots\ldots\ldots P_{n1} w_{n1}$$

Where, UTV refers to the urban thermal vulnerability, p refers to the value of the parameter and W refers to eh weight of the respective parameters respectively.

2.6. Statistical Analysis

In our study, we used correlation analysis and a linear regression model to discover the relationships between the parameters and to understand the impacts of the selected parameters on the UTV index. A close association exists between remote sensing indices and thermal patterns in cities. The biophysical indices play considerable roles in our understanding of the behaviors of thermal patterns. All the statistical analysis was carried out in SPSS software (version 22). The details of the research framework are presented in Fig. 2.

3. Results

From the LULC maps, we found that there was a substantial increase in built-up areas over the last 20 years in Jeddah (from 2000 to 2020) (Table 3 and Fig. 3). The results showed that from 2000 to 2020, the built-up area increased by approximately 50%, and open land and water bodies decreased by approximately 4.46% and 14.11%, respectively. From 2000 to 2020, vegetation cover increased by approximately 52.94%. In 2000, “open” was

the dominant land-cover type (83%), followed by built-up areas (14%), water bodies (6.5%), and vegetation. In 2020, open was the dominant land-cover type (74.96%) followed by built-up areas (22.12%), water bodies (2.74%), and vegetation (0.16%). Thus, among all the LULC types, built-up area and open land substantially increased (50.96% and 32.16%, respectively), and open land and vegetation cover decreased (13.24% and 11.48%).

There was also substantial spatial variation among the biophysical parameters depending on the section of the city analyzed. In the case of the NDVI, the mean value was 0.038, with maximum and minimum values of 0.431 and −0.238, respectively. The NDVI values were relatively higher along the coastal side of the city. The highest and lowest LSTs were 43.79 °C and 39.07 °C, respectively, with a mean LST of 41 .03 °C in 2021. The southeastern parts of the city were characterized by a relatively higher LST in comparison with other parts of the city. The LST value in southern-western parts of the city is mainly due to concentration of sands. The areas covered by built-up and sands are characterized by high LST over the city. In the case of wetness, we found a relatively high value along the coastline of the city. Furthermore, open and bare lands were characterized by higher LST, UTFVI, and TCI values (Fig. 4). The results also showed that there was also substantial spatial variation of NDVI, Wetness, NDMI and impervious indices (NDII, NDSI and NDISI). Southern and northern parts of the city are characterized by higher impervious surface as compared to other parts of the city.

In this study, we have developed UTV maps by using biophysical parameters for the year 2021, and by using PCA- and fuzzy-based methods. From both models, we identified similar spatial patterns of urban thermal vulnerability. Through our results, we found that the southeastern parts of the city were characterized as being at a very-high risk of thermal vulnerability. As per the fuzzy-AHP model, we also characterized the northeastern part of the city as having very poor urban thermal conditions. Furthermore, we characterized the western and central parts of the city as having poor UTV (Fig. 5).

UTV has been categorized into five classes: very poor, poor, average, good, and very good. Through our results, we identified more than 90% of the total area as having poor and very poor UTV. In the PCA-based model, we identified 73.64% and 20.12% of the total area as having poor and very poor UTV, respectively. However, with the fuzzy- AHP-based model, we found that approximately 57.29% and 40.56% of the total area came under the poor and very poor thermal vulnerable classes, respectively. We identified the smallest proportions of the areas as belonging to the very good and good UTV classes (Fig. 6).

We found that the LST (r = 0.590) (Fig. 7.a) and UTFVI (r = 0.927) (Fig. 7.g) had strong correlations with thermal vulnerability. Moreover, we found that the wetness (r = −0.892) (Fig. 7.b), NDVI (r = −0.052) (Fig. 7.d), and NDMI (r = −0.663) (Fig. 7.e) had strong negative correlations with thermal vulnerability (Fig. 7). Thus, from the correlation results, we discerned that the LST and UTFVI positively influenced, and NDVI, NDMI, and wetness negatively influenced, the thermal environment in the city. In our regression results, we found that the NDISI, LST, and wetness had a significant impact on UTV (R^2 = 0.943) (Fig. 7. g).

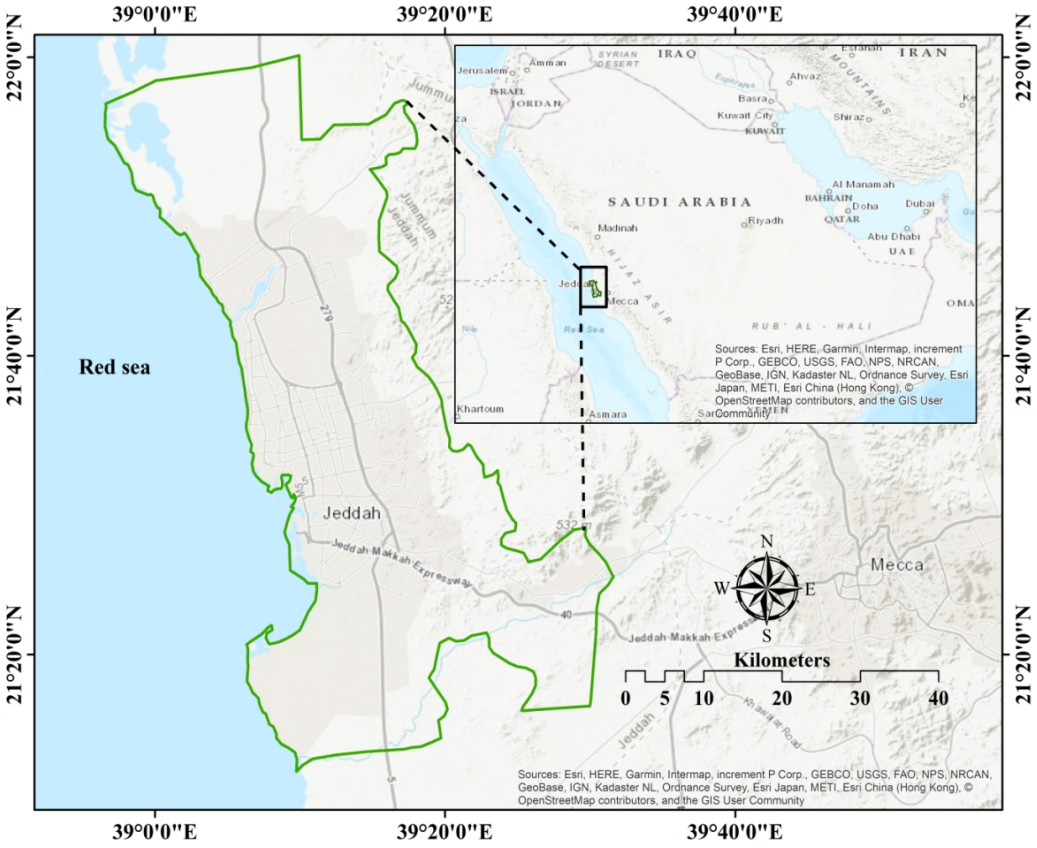

Fig. 1. Location map of the study area.

Table 1. Details of the datasets used in this study.

Satellite	Sensor	Spatial resolution (m)	Path and Row	Acquisition Date
LANDSAT 5	TM	30	170/045	30/09/2000
LANDSAT 8	OLI	30	170/045	16/09/2021

Table 2. Indices used in this study.

Indices	Equation	Description

NDVI	(NIR-Red/NIR+ Red) or (Band 5- Band 4/ band 5 + Band 4)	Band 4 refers to the Red band abd Band 5 refers to the Near Infrared band.
NDMI	(NIR- SWIR1)/ (NIR+SWIR1) (Band 5- Band 6/Band 5+ Band 6)	NIR (near infrared) refers to the band 5 and SWIR1(shortwave infrared) refers to the Band 6
NDII	(VIS- TIR1/ VIS+ TIR1)	VIS refers to the visible bands (2, 3, and 4), and TIR1 refers to the thermal infrared band 10 of LANDSAT 8.
NDSI	$\frac{SWIR1 - NIR}{SWIR1 + NIR}$	SWIR1(shortwave infrared) refers to the Band 6 and NIR (near infrared) refers to the band 5
NDISI	$\frac{TIR1 - \frac{W1 + NIR + + SWIR1}{3}}{TIR1 + \frac{W1 + NIR + SWIR1}{3}}$	TIR1 refers to the thermal infrared band 8 of LANDSAT 8; W1 refers to the water index; NIR refers to the band 5 (near infrared band) and SWIR1 refer to the Band 6 (shortwave infrared band)
UTFVI	$\frac{T_{a-T_m}}{SD}$	Ta refers to the actual LST, Tm refers to the mean LST and SD refers to the standard deviation.
TCI	$\frac{LST_{-LST_{min}}}{LST_{max} - LST_{min}} \times 100$	LST refers to the observed LST, LST_{min} and LST_{max} refers to the minimum and maximum LST from the entire area.
LST	$LST = T/1 + (\lambda T/\rho) \ln$	BT refers to the brightness temperature; W refers to the wavelength of the emitted radiance.

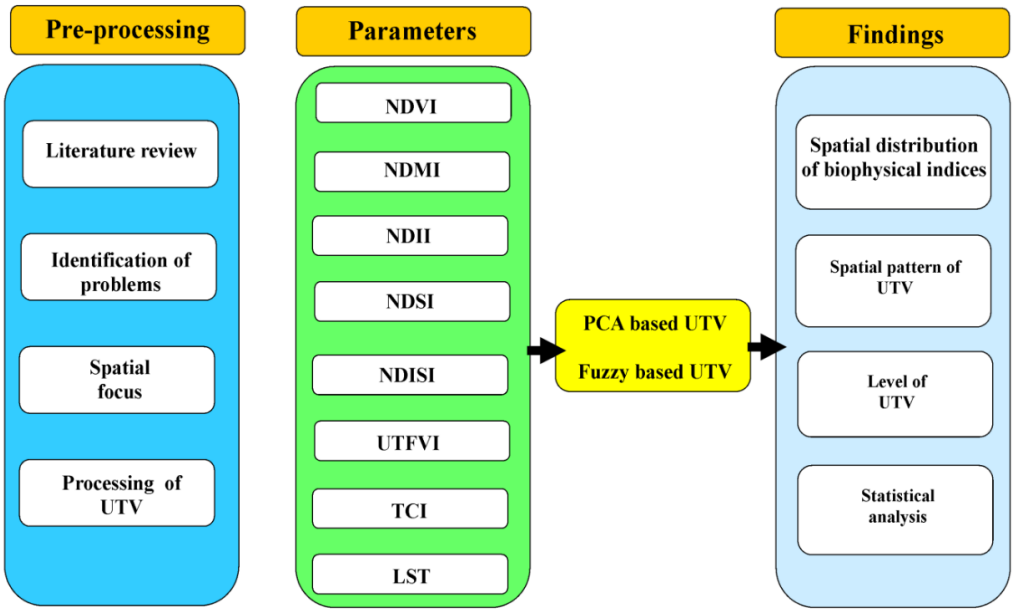

Fig. 2. Research framework used in this study.

Table 3. LULC dynamics in Jeddah Megacity (KM^2).

LULC types	2000	%	2021	%
Built up	30.86	14.05	46.58	22.12
Open land	181.91	82.85	157.82	74.96
Water	6.54	2.98	5.78	2.75
Vegetation	0.26	0.12	0.35	0.16

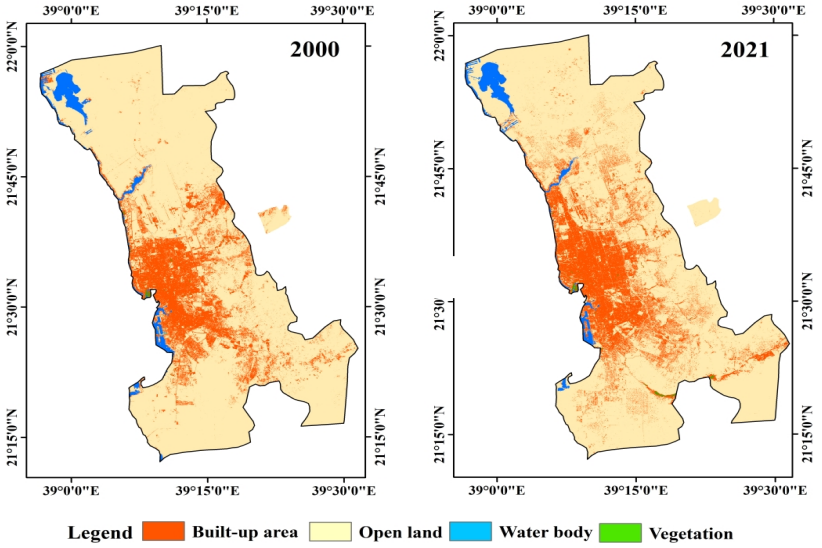

Fig. 3. Land use and land cover (LULC)-change map of the Jeddah megacity from 2000 to 2021.

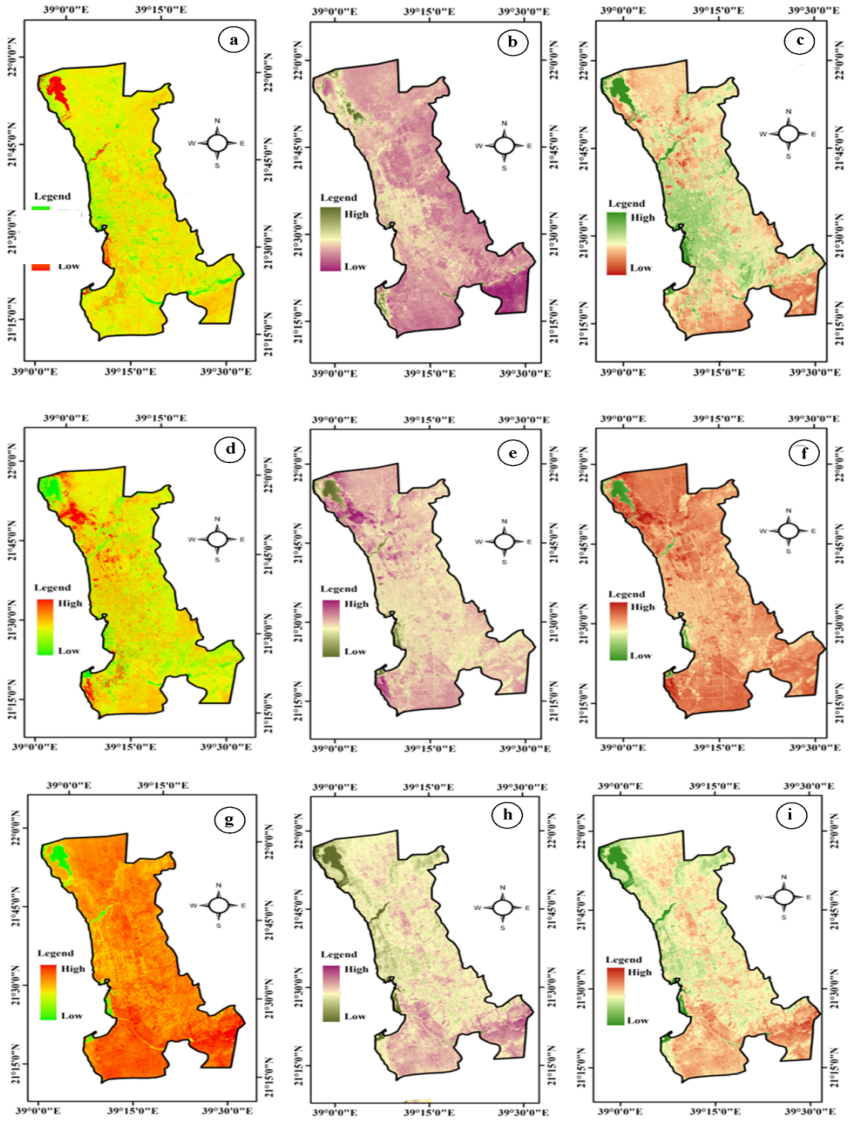

Fig. 4. Data layers: (a) NDVI, (b) wetness, and (c) NDMI (d) NDII, (e) NDSI (f) NDISI (g) LST, (h) UTFVI, and (i) TCI (2021).

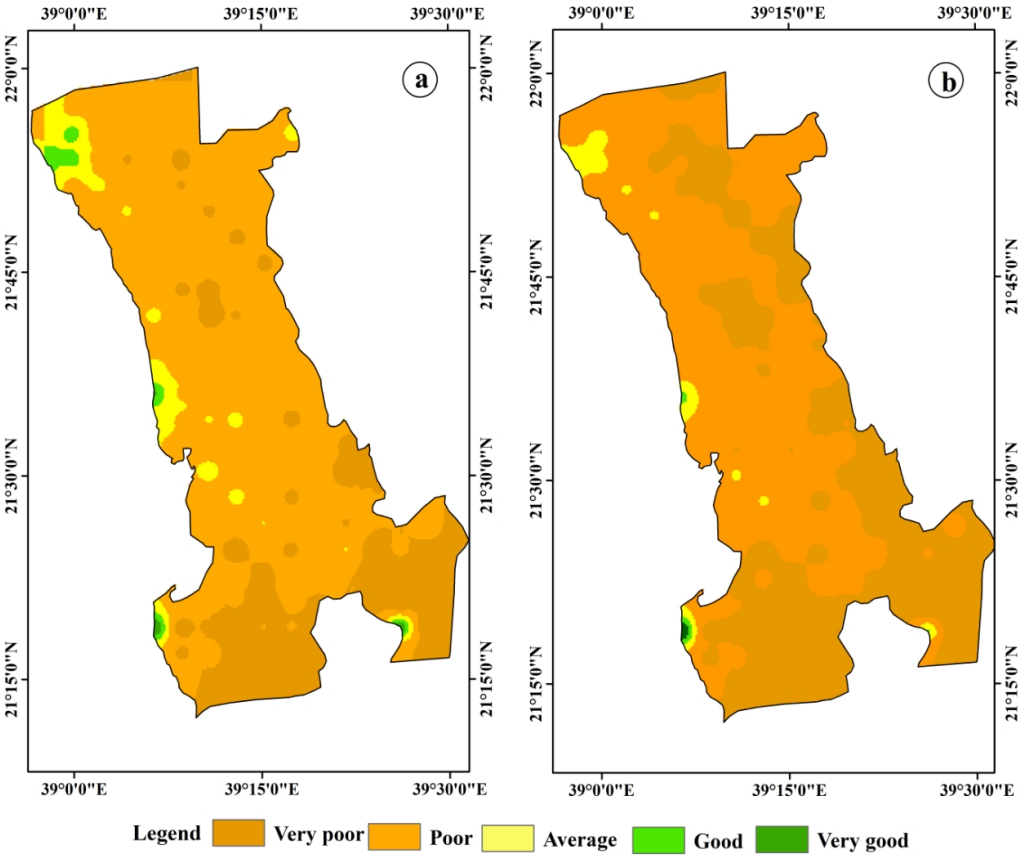

Fig. 5. UTV index: (a) PCA-based and (b) fuzzy-AHP-based.

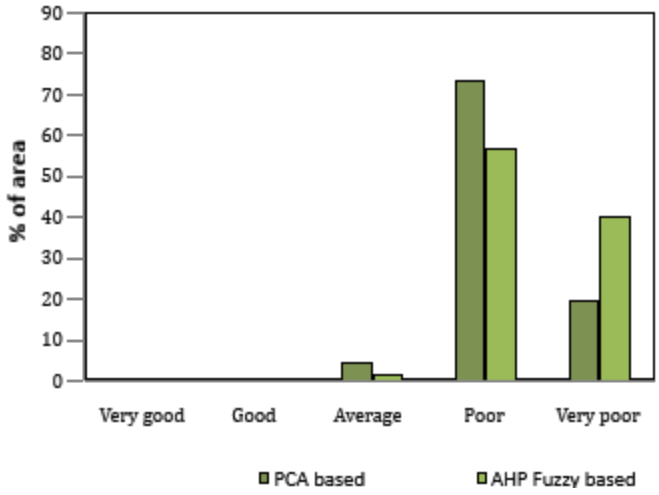

Fig. 6. Percentage of the area with various UTV levels.

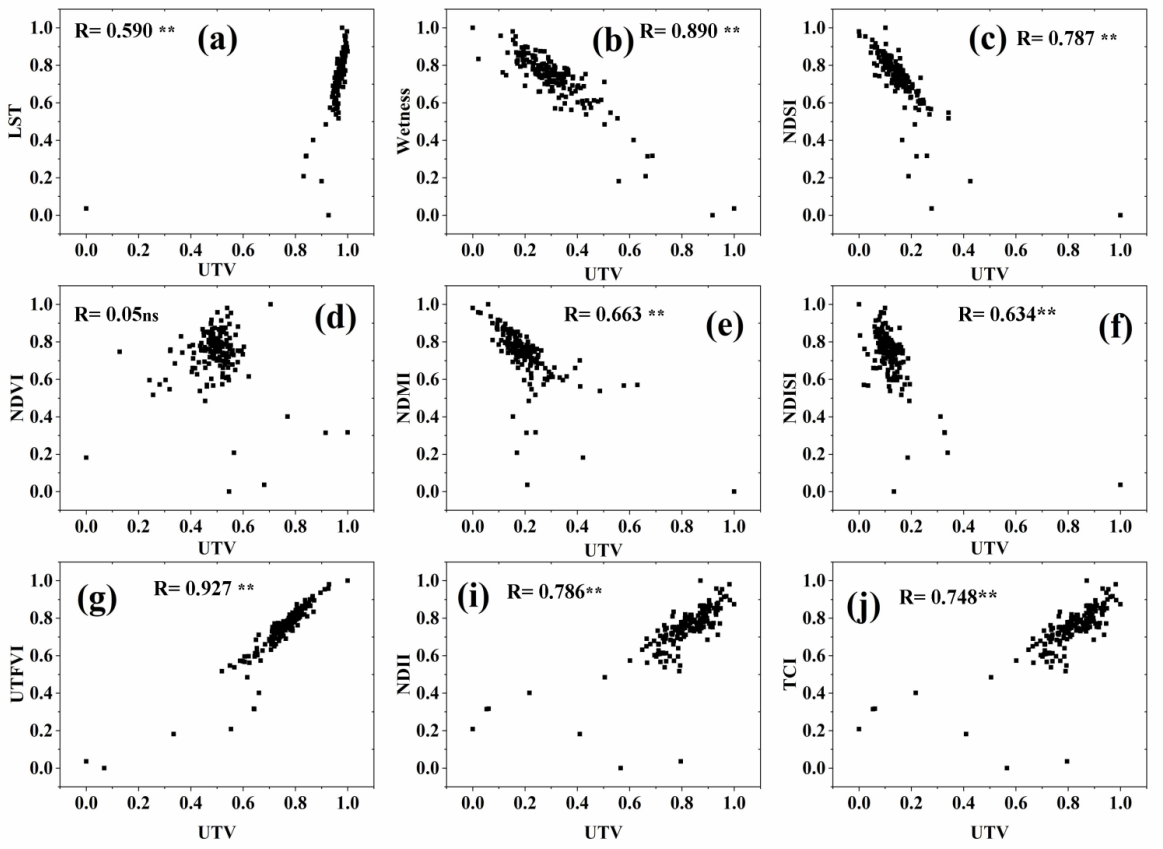

** Correlation is significant at the 0.01 level. 'ns 'means not sign.

Fig. 7. Correlations of UTV with the remote sensing indices.

4. Discussion

Urbanization has produced serious environmental problems due to the rapid transformations of pervious to impervious surface areas [82, 83]. The physical properties of the surface area, such as vegetation cover and how built-up it is highly sensitive to LST [84, 85]. Environmental temperatures increase in parallel with rising LST [86, 87, 88]. Thus, the increase in LST largely affects human thermal comfort, particularly for those people living under socio-economic stresses [89, 90], resulting in heat-related diseases and creating energy and water demands. Our findings showed that biophysical properties, such as the NDVI, built-up (NDBI), and water (NDWI) indices, highly affected the LST and triggered heat vulnerability. In our study, we found that the southern, southeastern, and middle sections of Jeddah were highly vulnerable to heat in comparison with other areas in the city. These areas are highly vulnerable to heat due to their mainly dry surfaces, lack of vegetation cover, and the presence of sand. The results of our study showed that land-use and land-cover types largely influenced the patterns of heat vulnerability (Appendix A2). The LST, which promotes heat vulnerability, rises with increasing proportions of impervious surfaces and decreasing surface wetness and vegetation cover [91, 92]. For example, thermal vulnerability is high in the south-eastern parts of the megacity and this is

because of the presence of bare or open land (such as deserts lands). A thermal vulnerability mapping assessment is urgently required to ensure sustainable urban landscape planning, thereby reducing human health risks. Effective measures to tackle climate change are needed. The rapid increase in LST due to the conversion from pervious to impervious surfaces is one of the major drivers of deteriorating thermal comfort levels in cities. In this context, a nature-based solution is a beneficial and effective option to reduce heat stress in cities [93, 94, 95]. Particularly, in Saudi Arabia, cities are facing extreme heat waves during the summer, which result in risks to human health. Therefore, to mitigate heat stress, nature-based solutions must be integrated into decision-making frameworks. In this context, urban greening must be promoted and integrated into decision making framework. Development of urban green spaces in open spaces, roads, corridors must be introduced. According to Sailor [96], the UHI effect can be overcome in two ways: First, the albedo of urban surface areas must be increased. This is because low-albedo roofing materials, such as dark roofs, help with absorbing heat from sunlight and make houses relatively warmer [97]. Few UHI mitigation strategies reduce heat stress in urban areas, though the application of light roofing colors can reduce temperatures. Second, an increase in vegetation cover in urban areas can considerably affect microclimatic conditions [98]. The green coverage across cities can be increased through tree-planting initiatives by local government bodies. Vegetation cover considerably reduces the temperature by lowering evapotranspiration levels [99], and directly impacts the UHI effect because of CO_2 absorption [100, 101]. Therefore, planners and policy makers must urgently adopt strategies for the mitigation of climate and UHI effects.

4.1. Factors Affecting Thermal Vulnerability

LULC types have significant impact on the thermal vulnerability. In previous piece of literatures, it was well documented that are areas covered with impervious surface, particularly built-up areas were characterized by relatively higher thermal vulnerability [102, 103]. On the other hand, the areas with higher vegetation and water coverage were characterized by lower thermal vulnerability [103]. It clearly denoted the fact that the composition of the surface has significant impact on the thermal heterogeneity in an urban area [104, 105]. In this study also, from the spatial maps of thermal vulnerability, it was clearly visible that the areas cover with built-up areas and open lands were characterized by higher thermal vulnerability. Thus, the findings of the study were similar to other studies.

Apart from LULC types, socio-demographic and physical factors plays significant role in the spatial heterogeneity of thermal vulnerability. For example, Reid et al. [106] carried out a study considering ten socio-demographic factors and found that substantial spatial variability in thermal vulnerability. Another study was carried out by Johnson et al. [107] developing a heat vulnerability index from 25 socioeconomic and environmental factors.

The findings showed that socio-economic factors significantly affected thermal vulnerability. Although this study has not considered socioeconomic and environmental factors directly, but from the spatial maps, it was well recognized that the urban areas were also highly vulnerable to thermal vulnerability. Thus, it can be stated that socio-economic and environmental factors plays significant role in determining thermal vulnerability.

5. Conclusions

In our study, we aimed to develop spatial heat vulnerability mapping in a desert megacity in Saudi Arabia by using remote-sensing indices. The results showed that most of the areas in Jeddah come under the high and very high thermal vulnerability categories. Particularly, the north, eastern, and southeastern parts of the city are relatively vulnerable to heat. The findings also showed that 73.64% (as per PCA based model) and 57.29% (Fuzzy-AHP model) areas were identified under very high vulnerable zones. LST (r = 0.590) and UTFVI (r = 0.927) had a strong positive correlation with thermal vulnerability. On the other hand, wetness (r = -0.892) NDVI (r = -0.052) and NDMI (r = -0.663) had negative correlation with thermal vulnerability, respectively. Though this study has significant role in understanding the spatial pattern of the thermal vulnerability in Jeddah and it may be very helpful for policy implications to the planners and policy makers. Despite this, this study has few limitations and these limitations can be addressed in future studies. These are, firstly, in this study thermal vulnerability has been assessed for the year of 2021, no temporal analysis was carried out. Therefore, in future studies, the temporal analysis of thermal vulnerability could be done. Secondly, in this study, the remote sensing indices were have been used to develop thermal vulnerability mapping. The thermal vulnerability is affected by a number such as factors socio-demographic factors [106], socio-physical factors [108]. Therefore, in the future studies, these factors should be taken into consideration while mapping thermal vulnerability. In spite of these limitations, this study has significant contribution towards policy perspectives to achieve urban environmental sustainability.

***Funding*:** This research received no external funding.

***Institutional Review Board Statement*:** Not applicable.

***Data Availability Statement*:** The data presented in this study are available on request from the corresponding author. The data are not publicly available due to privacy reasons.

***Conflicts of Interest*:** The authors declare no conflict of interest.

References

[1] **Xiang, Z.; Qin, H.; He, B.J.; Han, G.** and **Chen, M.** Heat vulnerability caused by physical and social conditions in a mountainous megacity of Chongqing, *China. Sustain. Cities Soc.* 2022, **80**, 103792.

[2] **Aubrecht, C.** and **Özceylan, D.** Identification of heat risk patterns in the U.S. National Capital Region by integrating heat stress and related vulnerability. *Environ. Int.* 2013, **56**, 65–77.

[3] **Mushore, T.D.; Mutanga, O.; Odindi, J.** and **Dube, T.** Determining extreme heat vulnerability of Harare Metropolitan City using multispectral remote sensing and socio-economic data. *J. Spat. Sci.* 2018, **63**, 173–191.

[4] **Quan, Q., Gao, S., Shang, Y.** and **Wang, B.** (2021). Assessment of the sustainability of Gymnocypriseckloni habitat under river damming in the source region of the Yellow River. *Science of the Total Environment*, **778**, 146312.

[5] **Zhang, K., Wang, S., Bao, H.** and **Zhao, X.** (2019). Characteristics and influencing factors of rainfall-induced landslide and debris flow hazards in Shaanxi Province, China. *Natural hazards and earth system sciences*, **19**(1), 93-105.

[6] **Wamsler, C.; Brink, E.** and **Rivera, C.** Planning for climate change in urban areas: From theory to practice. *J. Clean. Prod*. 2013, **50**,68–81.

[7] **Wolf, T.; McGregor, G.** The development of a heat wave vulnerability index for London, United Kingdom. *Weather. Clim. Extrem*. 2013, **1**, 59–68.

[8] **He, C.C.; Su, X.Q.; Bu, X.Q.** and **Xie,** Urbanization and Environmental Sustainable Development. Advanced Materials Research; *Trans Tech Publications Ltd*.: 2015; **1092**, pp.1629–1633.

[9] **Liang, L.; Wang, Z.** and **Li, J.,** The effect of urbanization on environmental pollution in rapidly developing urban agglomerations. *J. Clean. Prod*. 2019, **237**, 117649.

[10] D**.X. Tran, F.** and **Pla, P.**, Latorre-Carmona, S.W. Myint, M. Caetano, H.V. Kieu, Characterizing the relationship between land use land cover change and land surface temperature, *ISPRS J. Photogramm. Remote Sens*. **124** (2017) 119–132.

[11] **Fu, Peng** and **Qihao Weng**. "A time series analysis of urbanization induced land use and land cover change and its impact on land surface temperature with Landsat imagery." *Remote Sensing of Environment* **175** (2016): 205-214.

[12] **Li, B.; Chen, D.; Wu, S.; Zhou, S.; Wang, T.** and **Chen, H.,** Spatio-temporal assessment of urbanization impacts on ecosystem ser-vices: Case study of Nanjing City, *China. Ecol. Indic.* 2016, **71**, 416–427. https://doi.org/10.1016/j.ecolind.2016.07.017.

[13] **Sadiq Khan, M.; Ullah, S.; Sun, T.; Rehman, A.U.R.** and **Chen, L.**, Land-use/land-cover changes and its contribution to urban heat Island: A case study of Islamabad, *Pakistan. Sustainability* 2020, **12**, 3861.

[14] **Zhang, Y.** and **Sun, L.** Spatial-temporal impacts of urban land use land cover on land surface temperature: Case studies of two Canadian urban areas. Int. *J. Appl. Earth Obs. Geoinf*. 2019, **75**, 171-181.

[15] **Wang, S., Zhang, K., Chao, L., Li, D., Tian, X., Bao, H., ...** and **Xia, Y.** (2021). Exploring the utility of radar and satellite-sensed precipitation and their dynamic bias correction for integrated prediction of flood and landslide hazards. *Journal of Hydrology*, **603**, 126964.

[16] **Yue, Z., Zhou, W.** and **Li, T.** (2021). Impact of the Indian Ocean dipole on evolution of the subsequent ENSO: Relative roles of dynamic and thermodynamic processes. *Journal of Climate*, **34**(9), 3591-3607.

[17] **Li W., Cao Q., Lang K.** and **Wu J.** Linking potential heat source and sink to urban heat island: Heterogeneous effects of landscape pattern on land surface temperature. *Sci Total Environ*. 2017 May **15**; 586:457-465.

[18] **Bokaie, M., Zarkesh, M.M., Arasteh, P.D.** and **Hosseini, A.** (2016). Assessment of Urban Heat Island based on the relationship between land surface temperature and Land Use/ Land Cover in Tehran. *Sustainable Cities and Society*, **23**, 94-104.

[19] **Buchin, O., Hoelscher, M. T., Meier, F., Nehls, T., & Ziegler, F.** (2016). Evaluation of the Health-Risk Reduction Potential of Countermeasures to Urban Heat Islands. *Energy Build*, **114**, 27-37.

[20] **Wong, Li Ping** and **Alias**, Haridah and Aghamohammadi, Nasrin and Aghazadeh, Sima and Sulaiman, Nik Meriam Nik (2017) Urban heat island experience, control measures and health impact: A survey among working community in the city of Kuala Lumpur. *Sustainable Cities and Society*, **35**. 660-668.

[21] **Ramakrishnan, Sayanthan , Wang, Xiaoming , Sanjayan, Jay** and **Wilson, John,** 2017. "Thermal performance of buildings integrated with phase change materials to reduce heat stress risks during extreme heatwave events," *Applied Energy, Elsevier,* **194**(C), pages 410-421.

[22] **Heaviside, C., Macintyre, H.** and **Vardoulakis, S.,** The Urban Heat Island: Implications for Health in a Changing Environment. *CurrEnvir Health Rpt* **4**, 296-305 (2017).

[23] **Ghobadi, A.; Khosravi, M.** and **Tavousi, T.**, Surveying of Heat waves Impact on the Urban Heat Islands: Case study, the Karaj City in Iran. *Urban Clim*. 2018, **24**, 600-615.

[24] **Ellena, M.; Breil, M.** and **Soriani, S.**, The heat-health nexus in the urban context: A systematic literature review exploring the socio-economic vulnerabilities and built environment characteristics. *Urban Clim*. 2020, **34**, 100676.

[25 **Theeuwes, N. E.** (2015). Urban heat: natural and anthropogenic factors influencing urban air temperatures. Wageningen University. https://edepot.wur.nl/360261.

[26] **Mushore, T.D.; Mutanga, O.; Odindi, J.** and **Dube, T.**, Assessing the potential of integrated Landsat 8 thermal bands, with the traditional reflective bands and derived vegetation indices in classifying urban landscapes. *Geocarto Int.* 2017, **32**, 886-899.

[27] **Alonso, L.** and **Renard, F.,** A Comparative Study of the Physiological and Socio-Economic Vulnerabilities to Heat Waves of the Population of the Metropolis of Lyon (France) in a Climate Change Context. *Int. J. Environ. Res. Public Health* 2020, **17**, 1004.

[28] **Imran, H. M., Hossain, A., Islam, A. K. M. S., Rahman, A., Bhuiyan, M. A., Paul, S.** and **Alam, A.,** (2021). Impact of land cover changes on land surface temperature and human thermal comfort in Dhaka City of Bangladesh. *Earth Systems and Environment*, **5**(3), 667-693.

[29] **Aslam, A.; Rana, I.A.** and **Bhatti, S.S.,** The Spatiotemporal Dynamics of Urbanisation and Local Climate: A Case Study of Islamabad, Pakistan. Environ. *Impact Assess. Rev*. 2021, **91**, 106666.

[30] **Zaki, S.A.; Othman, N.E.; Syahidah, S.W.; Yakub, F.; Muhammad-Sukki, F.; Ardila-Rey, J.A.; Shahidan, M.F.** and **Saudi, A.S.M.** Ef-fects of Urban Morphology on Microclimate Parameters in an Urban University Campus. *Sustainability* 2020, **12**, 2962.

[31] **Zaki, S.; Azid, N.; Shahidan, M.; Hassan, M.; Daud, M.M.; Abu Bakar, N.; Salim, S.A.Z.S.** and **Yakub, F.** Analysis of Urban Mor-phological Effect on the Microclimate of the Urban Residential Area of Kampung Baru in Kuala Lumpur Using a Geospatial Approach. *Sustainability* 2020, **12**, 7301.

[32] **Mushore, T. D., Odindi, J., Dube, T., Matongera, T. N.,** and **Mutanga, O.** (2017). Remote sensing applications in monitoring urban growth impacts on in-and-out door thermal conditions: *A review. Remote Sensing Applications: Society and Environment*, **8**, 83-93.

[33] **Xu, H., Wang, Y., Guan, H., Shi, T.** and **Hu, X.** (2019). Detecting ecological changes with a remote sensing based ecological index (RSEI) produced time series and change vector analysis. *Remote Sensing*, **11**(20), 2345.

[34] **Xu, L., Liu, X., Tong, D., Liu, Z., Yin, L.** and **Zheng, W.** (2022). Forecasting Urban Land Use Change Based on Cellular Automata and the PLUS Model. *Land*, **11**(5), 652.

[35] **Zhao, M., Zhou, Y., Li, X., Cheng, W., Zhou, C., Ma, T., ...** and **Huang, K.** (2020). Mapping urban dynamics (1992–2018) in Southeast Asia using consistent nighttime light data from DMSP and VIIRS. *Remote Sensing of Environment*, **248**, 111980.

[36] **Inostroza L., Palme M.** and **de la Barrera F.** (2016) A Heat Vulnerability Index: Spatial Patterns of Exposure, Sensitivity and Adaptive Capacity for Santiago de Chile. *PLoS ONE* **11**(9): e0162464.

[37] **Zuhra, Syeda Samee**, **et al**. "Appraisal of the heat vulnerability index in Punjab: a case study of spatial pattern for exposure, sensitivity, and adaptive capacity in megacity Lahore, Pakistan." *International journal of biometeorology*. **63**,12 (2019): 1669-1682

[38] **Estoque, Ronald C., et al**. "Effects of landscape composition and pattern on land surface temperature: An urban heat island study in the megacities of Southeast Asia." *The Science of the total environment* **577** (2017): 349-359.

[39] **Tran, D.X.; Pla, F.; Latorre-Carmona, P.; Myint, S.W.; Gaetano, M.** and **Kieu, H.V.** Characterizing the relationship between land use land cover change and land surface temperature. *ISPRS J. Photogramm. Remote Sens.* 2017, **124**, 119–132.

[40] **De Almeida, C.R.; Teodoro, A.C.** and **Gonçalves, A.** Study of the Urban Heat Island (UHI) Using Remote Sensing Da-ta/Techniques: *A Systematic Review. Environments* 2021, **8**, 105.

[41] **Li, X.; Liu, T.; Lin, L.; Song, T.; Du, X.; Lin, H.; Xiao, J.; He, J.; Liu, L.; Zhu, G.; et al**. Application of the analytic hierar-chy approach to the risk assessment of Zika virus disease transmission in Guangdong Province, *China. BMC Infect Dis* **17**, 65 (2017).

[42] **Peng, J.; Jia, J.; Liu, Y.; Li, H.** and **Wu, J.,** Seasonal contrast of the dominant factors for spatial distribution of land surface tem-perature in urban areas. *Remote Sens. Environ.* 2018, **215**, 255–267.

[43] **Chow, W.T.L.; Volo, T.J.; Vivoni, E.R.; Jenerette, G.D.** and **Ruddell, B.L.** Seasonal dynamics of a suburban energy balance in Phoenix, Arizona. *Int. J. Clim*. 2014, **34**, 3863–3880.

[44] **Templeton, N. P., Vivoni, E. R., Wang, Z.-H.** and **Schreiner-McGraw, A. P. (**2018), Quantifying water and energy fluxes over different urban land covers in Phoenix, *Arizona. J. Geophys. Res*., **123**, 2111–2128.

[45] **Myint, S.W.; Zheng, B.; Talen, E.; Fan, C.; Kaplan, S.; Middel, A.; Smith, M.; Huang, H.-P.** and **Brazel, A.** (2015). Does the spatial arrangement of urban landscape matter? Examples of urban warming and cooling in Phoenix and Las Vegas. *Ecosystem Health and Sustainability*.

[46] **Li, Y., Du, L.** and **Wei, D.** (2021). Multiscale CNN based on component analysis for SAR ATR. *IEEE Transactions on Geoscience and Remote Sensing*, **60**, 1-12.

[47] **Tian, H., Wang, Y., Chen, T., Zhang, L.** and **Qin, Y.** (2021). Early-Season Mapping of Winter Crops Using Sentinel-2 Optical Imagery. *Remote Sensing*, **13**(19), 3822.

[48] **Meehl G. A.** and **Tebaldi C.,** More intense, more frequent, and longer lasting heat waves in the 21st century. *Science* **305**, 994(2004).

[49] **Vautard, R.; Yiou, P.; D'Andrea, F.; de Noblet, N.; Viovy, N.; Cassou, C.; Polcher, J.; Ciais, P.; Kageyama, M.** and **Fan, Y.** (2007) Summertime european heat and drought waves induced by wintertime mediterranean rainfall deficitGeophys. *Res. Lett*. **34**.

[50] **Huth, R.; Kysely, J.** and **Pokorna, L.** A GCM simulation of heat waves, dry spells, and their relationships to circulation. *Climatic Change* 2000, **46**, 29–60.

[51] **Lemonsu, A., Beaulant, A.L., Somot, S.** and **Masson, V**. (2014) Evolution of heat wave occurrence over the Paris basin (France) in the 21st century. *Clim Res* **61** :75-91.

[52] **Li, D.** and **Bou-Zeid, E.** Synergistic Interactions between Urban Heat Islands and Heat Waves: The Impact in Cities Is Larger than the Sum of Its Parts. *J. Appl. Meteorol. Climatol.* 2013, **52**, 2051–2064.

[53] **Basara, J.B.; Basara, H.G.; Illston, B.G.** and **Crawford, K.C.** *The Impact of the Urban Heat Island during an Intense Heat Wave in Oklahoma City*. Adv. Meteorol. 2010.

[54] **Leal Filho, W., Echevarria Icaza, L., Neht, A., Klavins, M.** and **Morgan, E. A.** (2018). Coping with the impacts of Urban Heat Islands A literature based study on understanding urban heat vulnerability and the need for resilience in cities in a global climate change context. *Journal of Cleaner Production*, **171**, 1140-1149.

[55] **Aljoufie, M.; Zuidgeest, M.; Brussel, M.** and **van Maarseveen, M.** Spatial-temporal analysis of urban growth and transportation in Jeddah City, Saudi Arabia. *Cities* 2013, **31**, 57–68.

[56] **Parvez, I. M., Aina, Y. A.** and **Balogun, A.** (2019). The influence of urban form on the spatiotemporal variations in land sur-face temperature in an arid coastal city. *Geocarto International*, **36**, 640–659.

[57] **Rahman, M.T.; Aldosary, A.S.** and **Mortoja, M.G.** Modeling Future Land Cover Changes and Their Effects on the Land Surface Temperatures in the Saudi Arabian Eastern Coastal City of Dammam. *Land* 2017, **6**, 36.

[58] **Harry, C.** (2015) Climate economics: economic analysis of climate change and climate policy, edited by Richard S. J. Tol. Published by Edward Elgar, Cheltenham, UK, 2014, pp. 208 pages, ISBN: 178 254 591 3. *Aust J Agric Resour Econ* **59**(2).

[59] **Wells, M. L., Trainer, V. L., Smayda, T. J., Karlson, B. S., Trick, C. G., Kudela, R. M., ...** and **Cochlan, W. P.** "Harmful algal blooms and climate change: Learning from the past and present to forecast the future." *Harmful algae*. **49** (2015): 68-93.

[60] **Addas, A., Maghrabi, A.** and **Goldblatt, R.** (2021). Public open spaces evaluation using importance-performance analysis (IPA) in Saudi Universities: the case of King Abdulaziz University, Jeddah. *Sustainability*, **13**(2), 915.

[61] **Xiang, Z., Qin, H., He, B. J., Han, G.** and **Chen, M.** (2022). Heat vulnerability caused by physical and social conditions in a mountainous megacity of Chongqing, China. *Sustainable Cities and Society*, **80**, 103792.

[62] **Hua, J., Zhang, X., Ren, C., Shi, Y.** and **Lee, T. C.** (2021). Spatiotemporal assessment of extreme heat risk for high-density cit-ies: A case study of Hong Kong from 2006 to 2016. *Sustainable cities and society*, **64**, 102507.

[63] **Baig, M. H. A., Zhang, L., Shuai, T., & Tong, Q**. (2014). Derivation of a tasselled cap transformation based on Landsat 8 at-satellite reflectance. *Remote Sensing Letters*, **5**(5), 423-431.

[64] **Mijani, N., Alavipanah, S. K., Firozjaei, M. K., Arsanjani, J. J., Hamzeh, S.** and **Weng, Q.** (2020). Modeling outdoor thermal comfort using satellite imagery: A principle component analysis-based approach. *Ecological Indicators*, **117**, 106555.

[65] **Abdi, H.** and **Williams, L. J.** (2010). Principal component analysis. *Wiley interdisciplinary reviews: computational statistics*, **2**(4), 433-459.

[66] **Maiti, S., Jha, S. K., Garai, S., Nag, A., Bera, A. K., Paul, V., ...** and **Deb, S. M.** (2017). An assessment of social vulnerability to climate change among the districts of Arunachal Pradesh, India. *Ecological Indicators*, **77**, 105-113.

[67] **Abson, D.J.; Dougill, A.J.** and **Stringer, L.C.** Using principal component analysis for information-rich socio-ecological vulnera-bility mapping in Southern Africa. *Appl. Geogr*. 2020, **35**, 515–524.

[68] **Tang, Y.; Feng, F.; Guo, Z.; Feng, W.; Li, Z.; Wang, J.; Sun, Q.; Ma, H.** and **Li, Y.** Integrating principal component analysis with sta-tistically-based models for analysis of causal factors and landslide susceptibility mapping: A comparative study from the loess plateau area in Shanxi (China). *J. Clean. Prod*. 2020, **277**, 124159.

[69] **X. Sun, Y. Zhou, L. Yuan, X. Li, H. Shao,** and **X. Lu,** "Integrated decision-making model for groundwater potential evaluation in mining areas using the cusp catastrophe model and principal component analysis," *Journal of Hydrology: Regional Studies*, **37**, no. 3, Article ID 100891, 2021.

[70] **Yu, C.** and **Chen, J.**, Application of a GIS-Based Slope Unit Method for Landslide Susceptibility Mapping in Helong City: Compar-ative Assessment of ICM, AHP, and RF Model. *Symmetry-Basel* 2020, **12**, 1848.

[71] **Zhao, H.; Yao, L.; Mei, G.; Liu, T.** and **Ning, Y.**, A fuzzy comprehensive evaluation method based on AHP and entropy for land-slide susceptibility map. *Entropy* 2017, **19**, 396.

[72] **Mallick, J.; Khan, R.A.; Ahmed, M.; Alqadhi, S.D.; Alsubih, M.; Falqi, I.** and **Hasan, M.A.**, Modeling Groundwater Potential Zone in a Semi-Arid Region of Aseer Using Fuzzy-AHP and Geoinformation Techniques. *Water* 2019, **11**, 2656.

[73] **Kumar, R., Dwivedi, S. B.** and **Gaur, S.** (2021). A comparative study of machine learning and Fuzzy-AHP technique to groundwater potential mapping in the data-scarce region. *Computers & Geosciences*, **155**, 104855.

[74] **Liou, Y.A.; Nguyen, A.K.** and **Li, M.H.**, Assessing spatiotemporal eco-environmental vulnerability by Landsat data. *Ecol. Indic*. 2017,**80**, 52–65.

[75] **Guo, X.** and **Kapucu, N.**, Assessing Social Vulnerability to Earthquake Disaster Using Rough Analytic Hierarchy Process Meth-od: A Case Study of Hanzhong City, *China. Saf. Sci*. 2020, **125**, 104625.

[76] **Giri, M., Bista, G., Singh, P. K.** and **Pandey, R.** (2021). Climate change vulnerability assessment of urban informal settlers in Nepal, a least developed country. *Journal of Cleaner Production*, **307**, 127213.

[77] **Nazri Che, D.; Abu Hassan, A.; Zulkiflee Abd, L.** and **Rodziah, I.** Application of geographical informationsystem-based analyti-cal hierarchy process as a tool for dengue risk assessment. Asian Pac. *J. Trop. Dis.* 2016,**6**, 928–935.

[78] **Saaty, T.L.** (1988). What is the Analytic Hierarchy Process? In: Mitra, G., Greenberg, H.J., Lootsma, F.A., Rijkaert, M.J., Zimmermann, H.J. (eds) Mathematical Models for Decision Support. *NATO ASI Series*, **48**. Springer, Berlin, Heidelberg.

[79] **Sarkar, S., Parihar, S.M.** and **Dutta, A.** (2016). Fuzzy risk assessment modelling of East Kolkata Wetland Area: A remote sensing and GIS based approach. Environ. *Model. Softw*., **75**, 105-118.

[80] **Kim, S.** and **Park, S.** (2022). Heatwave Vulnerability Analysis of Construction Sites Using Satellite Imagery Data and Deep Learning. *KSCE Journal of Civil and Environmental Engineering Research*, **42**(2), 263–272.

[81] **Boori, Mukesh Singh**, **et al**. "Spatiotemporal ecological vulnerability analysis with statistical correlation based on satellite remote sensing in Samara, Russia." *Journal of environmental management*. **285** (2021): 112138.

[82] **Yang, K.; Pan, M.; Luo, Y.; Chen, K.; Zhao, Y.** and **Zhou, X.**, A time-series analysis of urbanization-induced impervious surface ar-ea extent in the Dianchi Lake watershed from 1988–2017. *Int. J. Remote. Sens*. 2019, **40**, 573–592.

[83] **Shi, L.; Ling, F.; Ge, Y.; Foody, G.M.; Li, X.; Wang, L.; Zhang, Y.; Du, Y.** Impervious surface change mapping with an uncer-taintybased spatial-temporal consistency model: A case study in Wuhan City using Landsat time-series datasets from 1987 to 2016. *Remote Sens*. 2017, **9**, 1148.

[84] **Mathew, A., Khandelwal, S.** and **Kaul, N.** (2016). Spatial and temporal variations of urban heat island effect and the effect of percentage impervious surface area and elevation on land surface temperature: Study of Chandigarh city, *India. Sustainable Cities and Society*, **26**, 264-277.

[85] **Guo, L., Liu, R., Men, C., Wang, Q., Miao, Y.** and **Zhang, Y.** (2019). Quantifying and simulating landscape composition and pattern impacts on land surface temperature: A decadal study of the rapidly urbanizing city of Beijing, China. *Science of the Total Environment*, **654**, 430-440.

[86] **Fei, W.; Zhihao, Q.; Caiying, S.; Lili, T.; Arnon, K.** and **Shuhe, Z.** An Improved Mono-Window Algorithm for Land Surface Tem-perature Retrieval from Landsat 8 Thermal Infrared Sensor Data. *Remote Sens*. 2015, **7**, 4268–4289.

[87] **Ward, K.; Lauf, S.; Kleinschmit, B.** and **Endlicher, W.,** "Heat waves and urban heat islands in Europe: A review of relevant driv-ers." *The Science of the total environment*. **569-570** (2016): 527-539.

[88] **Harun, Z., Reda, E., Abdulrazzaq, A., Abbas, A. A., Yusup, Y.** and **Zaki, S. A.** (2020). Urban heat island in the modern tropical Kuala Lumpur: Comparative weight of the different parameters. *Alexandria Engineering Journal*, **59**(6), 4475-4489.

[89] **Chen, L.; Wang, X.; Cai, X.; Yang, C.** and **Lu, X.** Seasonal Variations of Daytime Land Surface Temperature and Their Underlying Drivers over Wuhan, China. *Remote Sens*. 2021, **13**, 323.

[90] **Dissanayake, D.; Morimoto, T.; Murayama, Y.; Ranagalage, M.** and **Handayani, H.H.**, Impact of Urban Surface Characteristics and Socio-Economic Variables on the Spatial Variation of Land Surface Temperature in Lagos City, Nigeria. *Sustainability* 2019, **11**, 25.

[91] **Dutta, D.; Rahman, A.; Paul, S.** and **Kundu, A.,** Impervious surface growth and its inter-relationship with vegetation cover and land surface temperature in peri-urban areas of Delhi. *Urban Clim*. 2021, **37**, 100799.

[92] **Wang, C., Li, Y., Myint, S. W., Zhao, Q.** and **Wentz, E. A.** (2019) Impacts of spatial clustering of urban land cover on land surface temperature across Köppen climate zones in the contiguous United States. *Landscape and Urban Planning*, **192**, 103668.

[93] **Lafortezza, Raffaele**, **et al.**, "Nature-based solutions for resilient landscapes and cities." *Environmental research*. **165** (2018): 431-441.

[94] **Niki Frantzeskaki, Timon McPhearson, Marcus J Collier, Dave Kendal, Harriet Bulkeley, Adina Dumitru, Claire Walsh, Kate Noble, Ernita van Wyk, Camilo Ordóñez, Cathy Oke** and **László Pintér**, Nature-Based Solutions for Urban Climate Change Ad-aptation: Linking Science, Policy, and Practice Communities for Evidence-Based Decision-Making, *BioScience*, **69**(6), June 2019, Pages 455–466.

[95] **Wollmann, C. A., Hoppe, I. L., Gobo, J. P. A., Simioni, J. P. D., Costa, I. T., Baratto, J.,** and **Shooshtarian, S**. (2021). Ther-mo-hygrometric variability on waterfronts in negative radiation balance: A case study of balneárioCamboriú/SC, Brazil. *Atmosphere*, **12**(11), 1453.

[96] **Sailor, D. J.** (2006, January). Mitigation of urban heat islands-Recent progress and future prospects. In Paper presented on american meteorological society *6th symposium on the urban environment and forum on managing our physical and nat-ural resources.*

[97] **Akbari, H.** and **Kolokotsa, D.** (2016). Three decades of urban heat islands and mitigation technologies research. *Energy and buildings*, **133**, 834-842.

[98] **Wilmers, F.** (1988). *Green in urban climate. In Environmental Meteorology* (pp. 359-379). Springer, Dordrecht.

[99] **Eichelmann, E.; Hemes, K.S.; Knox, S.H.; Oikawa, P.Y.; Chamberlain, S.D.; Sturtevant, C.; Verfaillie,**

J. and **Baldocchi, D.D.** (2018) The effect of land cover type and structure on evapotranspiration from agricultural and wetland sites in the Sacramento–San Joaquin River Delta. *California Agricultural and Forest Meteorology* **256-257**:179–195.

[100] **Qiu, G.Y.; Zou, Z.; Li, X.; Li, H.; Guo, Q.; Yan, C.** and **Tan, S.,** Experimental studies on the effects of green space and evapotranspi-ration on urban heat island in a subtropical megacity in China. *Habitat Int*. 2017, **68**, 30–42.

[101] **Moghbel, M.** and **Salim, R.E.** Environmental benefits of green roofs on microclimate of Tehran with specific focus on air tem-perature, humidity and CO_2 content. *Urban Clim*. 2017, **20**, 46–58.

[102] **Henits, L., Mucsi, L.** and **Liska, C. M.** (2017). Monitoring the changes in impervious surface ratio and urban heat island inten-sity between 1987 and 2011 in Szeged, Hungary. *Environmental monitoring and assessment*, **189** (2), 1-13.

[103] **Yuan, F.** and **Bauer, M. E.** (2007). Comparison of impervious surface area and normalized difference vegetation index as in-dicators of surface urban heat island effects in Landsat imagery. *Remote Sensing of environment*, **106**(3), 375-386.

[104] **Estoque, R. C., Murayama, Y.** and **Myint, S. W.** (2017). Effects of landscape composition and pattern on land surface temper-ature: An urban heat island study in the megacities of Southeast Asia. *Science of the Total Environment*, **577**, 349-359.

[105] **Soydan, O.** (2020). Effects of landscape composition and patterns on land surface temperature: Urban heat island case study for Nigde, Turkey. *Urban Climate*, **34**, 100688.

[106] **Reid, C. E., O'neill, M. S., Gronlund, C. J., Brines, S. J., Brown, D. G., Diez-Roux, A. V.** and **Schwartz, J**. (2009). Mapping com-munity determinants of heat vulnerability. *Environmental health perspectives*, **117**(11), 1730-1736.

[107] **Johnson, D. P., Stanforth, A., Lulla, V.** and **Luber, G**. (2012). Developing an applied extreme heat vulnerability index utilizing socioeconomic and environmental data. *Applied Geography*, **35**(1-2), 23-31.

[108] **Xiang, Z., Qin, H., He, B. J., Han, G.** and **Chen, M.** (2022). Heat vulnerability caused by physical and social conditions in a mountainous megacity of Chongqing, *China. Sustainable Cities and Society*, **80**, 103792.

Appendix A

A1: Weights of the parameters

Parameter	Weight
Normalized difference Vegetation index (NDVI)	0.11
Normalized Difference Moisture Index (NDMI)	0.087
Normalized Difference Impervious Index (NDII)	0.14
Normalized Difference Soil Index (NDSI)	0.125
Normalized Difference Impervious Surface Index (NDISI)	0.102
Urban Thermal Field Variance Index (UTFVI)	0.132
Temperature Condition Index (TCI)	0.132
Land Surface Temperature (LST)	0.18

A2: Validation of the results

Fig. A1: The google earth images with the areas of low thermal vulnerability (left) and high thermal vulnerability (right).

رسم خرائط نقاط الضعف الحرارية الحضرية للتخفيف من آثار تغير المناخ: حالة من المدن الساحلية الكبرى بالمملكة العربية السعودية

أحمد المغربي

كلية العمارة والتخطيط، جامعة الملك عبد العزيز، جدة، المملكة العربية السعودية

amaghrabi84@gmail.com

المستخلص. يؤثر التوسع الحضري السريع بشكل كبير على خصائص الأسطح الحضرية من خلال استبدال المناظر الطبيعية بمساحات سطحية غير منفذة. تؤثر هذه التغييرات بشكل كبير على الخواص الحرارية للمناظر الطبيعية الحضرية وتزيد من كثافة الجزر الحرارية الحضرية (UHI) والضعف الحراري؛ ولذلك، فإن رسم خرائط الضعف الحراري للتخفيف من مخاوف الصحة العامة أمر ضروري. في هذه الدراسة، قمنا برسم خريطة الضعف الحراري لمدينة جدة الكبرى بالمملكة العربية السعودية، باستخدام تحليل المكونات الرئيسية (PCA)، ونموذج عملية التسلسل الهرمي التحليلي الغامض (fuzzy-AHP). لقد أجرينا أيضاً تحليلات الارتباط والانحدار لفهم العلاقات وتأثيرات مؤشرات الاستشعار عن بعد على الضعف الحراري. وأظهرت النتائج أنه خلال الفترة من 2000 إلى 2020، زادت الأراضي المبنية والمسطحات المائية والأراضي المفتوحة بنحو 50٪، و4,46٪، و14,11٪ على التوالي. لقد وجدنا أن الأجزاء الجنوبية الشرقية من المدينة كانت شديدة التأثر وفقاً لخريطة الضعف الحراري. في كلا النموذجين، تم وصف 73,64٪ (النموذج القائم على PCA) و57,29٪ (النموذج القائم على AHP الغامض) من المدينة على أنها مناطق معرضة للحرارة. في نتائج الارتباط الخاصة بنا، أظهرنا أن المعلمات البيئية، مثل الفرق الطبيعي للغطاء النباتي (NDVI) ومؤشرات الرطوبة (NDMI)، وكذلك البلل، لها ارتباطات سلبية مع الضعف الحراري الحضري، في حين أن الارتباطات لدرجة حرارة سطح الأرض (LST) كانت لها ارتباطات سلبية مع الضعف الحراري الحضري. وكان مؤشر تباين المجال الحراري الحضري (UTFVI) إيجابياً. وهكذا، قمنا في هذه الدراسة ببناء إطار فعال لاستراتيجيات التخفيف من آثار تغير المناخ التي يمكن استخدامها لتقليل التعرض للحرارة أو الحرارة في المناطق الحضرية.

الكلمات المفتاحية: الضعف الحراري، مدينة جدة الكبرى، تحليل المكونات الرئيسة، الصحة العامة، التخفيف من آثار المناخ.